Supporting Information

Resonance/off-resonance excitations: Implications on the thermal evolution of Eu^{3+} photoluminescence

Arnab De[1◦], Miguel A. Hernández-Rodríguez[2], Albano N. Carneiro Neto[2]*, Vivek Dwij[3], Vasant Sathe[3], Luís D. Carlos[2]*, Rajeev Ranjan[1]*

[1] Department of Materials Engineering, Indian Institute of Science, Bangalore-560012, India.

[2] Phantom-g, CICECO – Aveiro Institute of Materials, Physics Department, University of Aveiro, 3810-193, Aveiro, Portugal.

[3] UGC-DAE Consortium for Scientific Research, Indore, Devi Ahilya University Campus, Indore 452001, India.

◦ Present address: Department of Physics, Sungkyunkwan University, Suwon, Gyeonggi 16419, South Korea.

* Corresponding authors: lcarlos@ua.pt; albanoneto@ua.pt; rajeev@iisc.ac.in

Contents

S1. Orbital and Spin matrix elements

For an intraconfiguracional *f-f* transition between $|\psi J\rangle$ and $|\psi' J'\rangle$ states, the matrix elements $\langle\psi' J'\|\mathbf{L} + g_S\mathbf{S}\|\psi J\rangle$ can be separated into two contributions:

$$\langle\psi' J'\|\mathbf{L} + g_S\mathbf{S}\|\psi J\rangle = \langle\psi' J'\|\mathbf{L}\|\psi J\rangle + g_S\langle\psi' J'\|\mathbf{S}\|\psi J\rangle \tag{S1}$$

which can be calculated using the intermediate coupling wavefunctions.

For the orbital and spin angular momentum operators (**L** and **S**), the matrix elements become

$$\begin{aligned}\langle\psi' J'\|\mathbf{L}\|\psi J\rangle &= a'_1 a_1\langle\varphi'_1\|\mathbf{L}\|\varphi_1\rangle + a'_2 a_2\langle\varphi'_2\|\mathbf{L}\|\varphi_2\rangle + \cdots + a'_n a_n\langle\varphi'_n\|\mathbf{L}\|\varphi_n\rangle \\ &= \sum_n a'_n a_n\langle\varphi'_n\|\mathbf{L}\|\varphi_n\rangle\end{aligned} \tag{S2}$$

$$\begin{aligned}\langle\psi' J'\|\mathbf{S}\|\psi J\rangle &= a'_1 a_1\langle\varphi'_1\|\mathbf{S}\|\varphi_1\rangle + a'_2 a_2\langle\varphi'_2\|\mathbf{S}\|\varphi_2\rangle + \cdots + a'_n a_n\langle\varphi'_n\|\mathbf{S}\|\varphi_n\rangle \\ &= \sum_n a'_n a_n\langle\varphi'_n\|\mathbf{S}\|\varphi_n\rangle\end{aligned} \tag{S3}$$

where a_n and a'_n are the coefficients of Ofelt's wavefunctions [1]. $\psi = \varphi LS$ and $\psi' = \varphi' L' S'$ are the wavefunctions of the $|^{2S+1}L\rangle$ and $|^{2S'+1}L'\rangle$ states in the Russell-Saunders coupling.

Each matrix element involves the same (spectroscopic) terms (or states) element in the summation in Eqs. S2 and S3 are obtained as:

$$\begin{aligned}&\langle\varphi'_n L' S'\|\mathbf{L}\|\varphi_n LS\rangle \\ &= (-1)^{L+S+J+1}\sqrt{(2J+1)(2J'+1)L(L+1)(2L+1)}\begin{Bmatrix} J & 1 & J' \\ L & S & L\end{Bmatrix}\delta_{\varphi,\varphi'}\delta_{L,L'}\delta_{S,S'}\end{aligned} \tag{S4}$$

$$\begin{aligned}&\langle\varphi'_n L' S'\|\mathbf{S}\|\varphi_n LS\rangle \\ &= (-1)^{L+S+J'+1}\sqrt{(2J+1)(2J'+1)S(S+1)(2S+1)}\begin{Bmatrix} S & J & L \\ J' & S & 1\end{Bmatrix}\delta_{\varphi,\varphi'}\delta_{L,L'}\delta_{S,S'}\end{aligned} \tag{S5}$$

Apart from the *S* and *L* terms changing inside the squared root and the 6-*j* symbol, Eqs. S4 and S5 also differ in their *J* quantum number involved in the power of –1 term: the **L** operator depends on the initial *J* while the **S** on the final *J'* quantum number. This means that *S* and *L* in most cases can contribute with an opposite signal in the total $\langle\psi' J'\|\mathbf{L} + g_S\mathbf{S}\|\psi J\rangle$ matrix elements (Eq. S1). Therefore, since the selection rules on the *J* quantum number is $\Delta J = 0, \pm 1$ ($J = J' = 0$ excluded), it is not difficult to demonstrate that the $(-1)^{L+S+J+1} = (-1)^{L+S+J'+1}$ for $\Delta J = 0$ and $(-1)^{L+S+J+1} = -(-1)^{L+S+J'+1}$ for $\Delta J = \pm 1$.

Table S1 summarizes the coefficients from Ofelt's wavefunctions in the intermediate coupling scheme [1]. Table S2 shows the values of calculated $\langle{}^7F_{J+1}\|\mathbf{L} + g_S\mathbf{S}\|{}^7F_J\rangle$ matrix elements.

S2. Judd-Ofelt intensity parameters

Einstein's spontaneous emission coefficients ($A_{0\to J}$) for the intraconfigurational transitions $^5D_0 \rightarrow {}^7F_J$ transitions (J= 2 and 4) were obtained based on emission spectra (Figure S1(a,c)) by [2]:

$$A_{0\to J} = A_{0\to 1} \cdot \left(\frac{S_{0\to J}}{S_{0\to 1}}\right) \tag{S6}$$

where the quantities $S_{0\to 1}$ and $S_{0\to J}$ are the integrated luminescence intensities of the transitions $^5D_0 \rightarrow {}^7F_1$ and $^5D_0 \rightarrow {}^7F_J$ (J = 2, 4, and 6), respectively. In Eu(III)-based compounds, the $^5D_0 \rightarrow {}^7F_1$ transition is governed by the magnetic dipole mechanism [3,4]. Therefore, the radiative coefficient $A_{0\to 1}$ is used as an internal standard since it is insensitive to changes in the chemical environment of the first coordination shell around the Eu^{3+} ion [5].

$$A_{0\to 1} = \frac{4e^2(\omega_{0\to 1})^3 {n_r}^3}{3\hbar c^3} S_{md} \tag{S7}$$

where

$$S_{md} = {\mu_B}^2 \langle {}^5D_0 \| \mathbf{L} + g_S \mathbf{S} \| {}^7F_1 \rangle^2 \tag{S8}$$

is the magnetic dipole strength (in units of $esu^2 \cdot cm^2$) for the $^5D_0 \rightarrow {}^7F_1$ transitions. The reduced matrix elements $\langle {}^5D_0 \| \mathbf{L} + g_S \mathbf{S} \| {}^7F_1 \rangle$ is obtained according to the previous section. The $\omega_{0\to 1}$ is the angular frequency of the $^5D_0 \rightarrow {}^7F_1$ transition, μ_B is Bohr's magneton, c is the vacuum speed of light, and n_r is the refractive index of the medium ($n_r \approx 2.3$ for $CaTiO_3$ [6] and $n_r \approx 2.4$ for $BaTiO_3$ [7]).

Once the values of $A_{0\to J}$ for Eu^{3+} $^5D_0 \rightarrow {}^7F_{2,4}$ transitions are obtained, the experimental Judd-Ofelt intensity parameters (Ω_2, Ω_4) can be calculated by [8]:

$$\Omega_\lambda = \frac{3\hbar c^3 A_{0\to J}}{4e^2\omega^3 \chi \langle {}^7F_\lambda \parallel \boldsymbol{U}^{(\lambda)} \parallel {}^5D_0 \rangle^2} \tag{S9}$$

where $\chi = n_r({n_r}^2 + 2)^2/9$ is the Lorentz local field correction and $\langle {}^7F_\lambda \parallel \boldsymbol{U}^{(\lambda)} \parallel {}^5D_0 \rangle^2$ are the square reduced matrix elements with values 0.0032 and 0.0023 for λ = 2 and 4, respectively [9]. The values of Ω_2 and Ω_4 are in Table S3.

S3. Figures

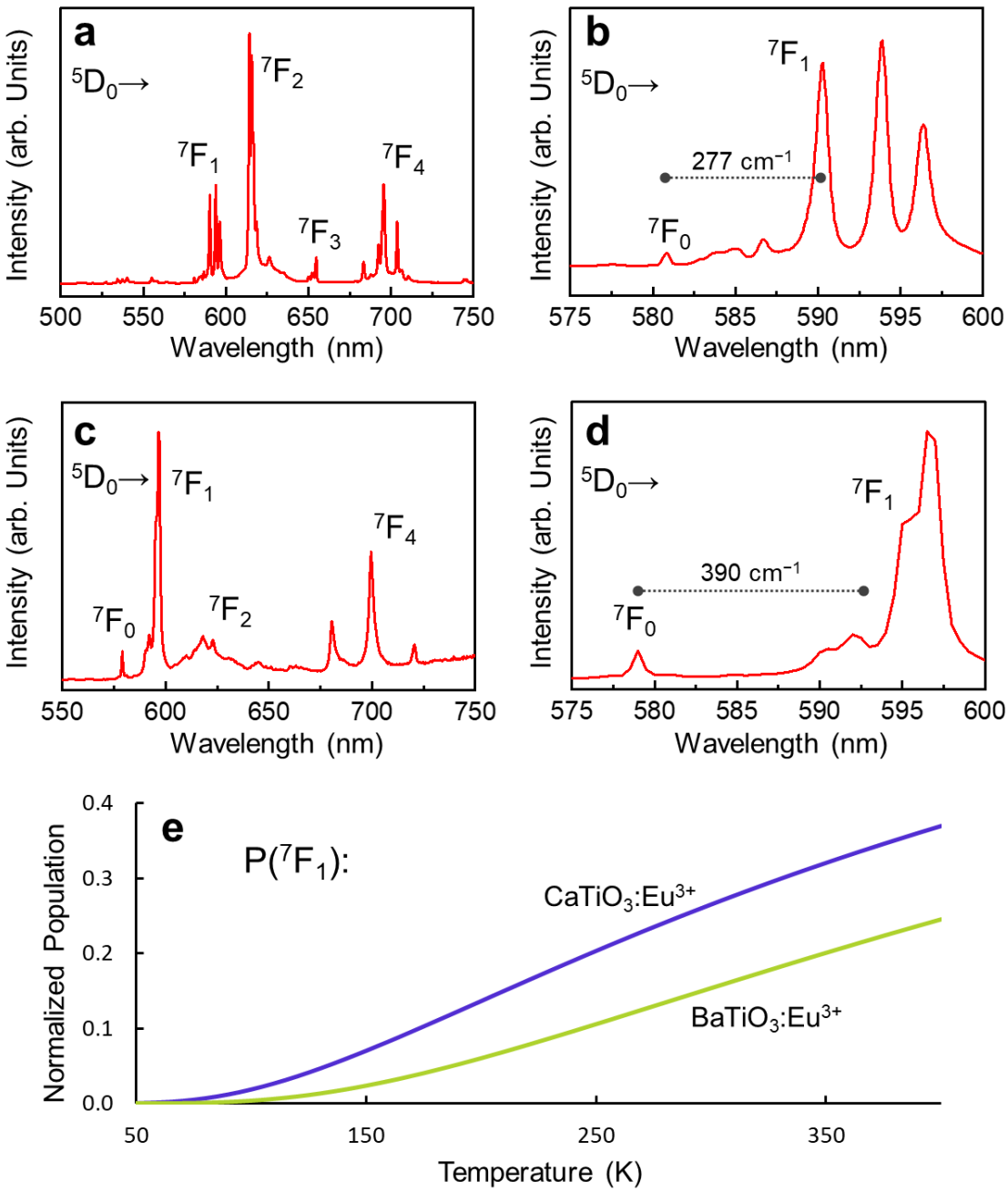

Figure S1. Room temperature emission spectra of (a) $CaTiO_3:Eu^{3+}$ and (c) $BaTiO_3:Eu^{3+}$ upon 397 nm excitation (lamp source). (b) and (d) are the magnificance of (a) and (c) in the $^5D_0\rightarrow{}^7F_{0,1}$ spectral range to obtain the $^7F_0$ and $^7F_1$ energy gap. The $CaTiO_3:Eu^{3+}$ presents a lower energy (ca. 277 cm^{-1}) in comparision to the $BaTiO_3:Eu^{3+}$ (ca. 390 cm^{-1}), leading to higher Boltzmann population (e) of the $^7F_1$ in $CaTiO_3:Eu^{3+}$.

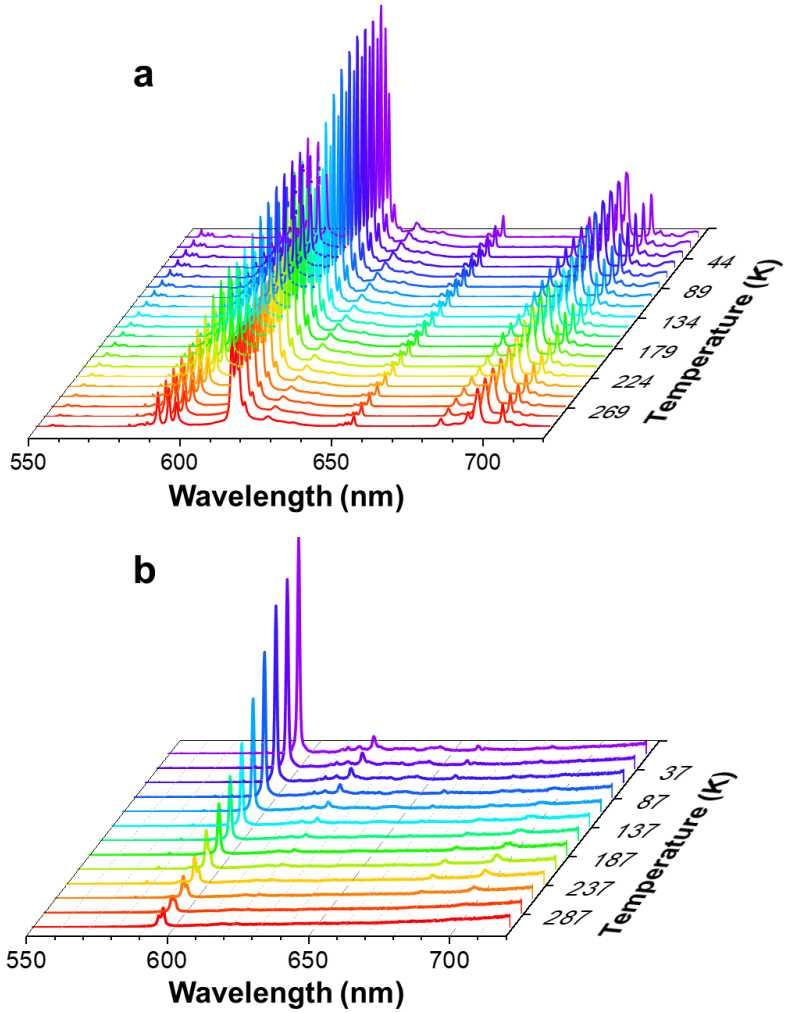

Figure S2. Temperature dependence of the emission spectra of (a) $CaTiO_3$:0.5Eu excited in-resonance at 465 nm (lamp source with the bandpass of ±6.6 nm). (b) Temperature dependence of the emission spectra of $BaTiO_3$:0.5Eu^{3+} excited in-resonance at 471.2 nm (lamp source with a bandpass of ±1.5 nm).

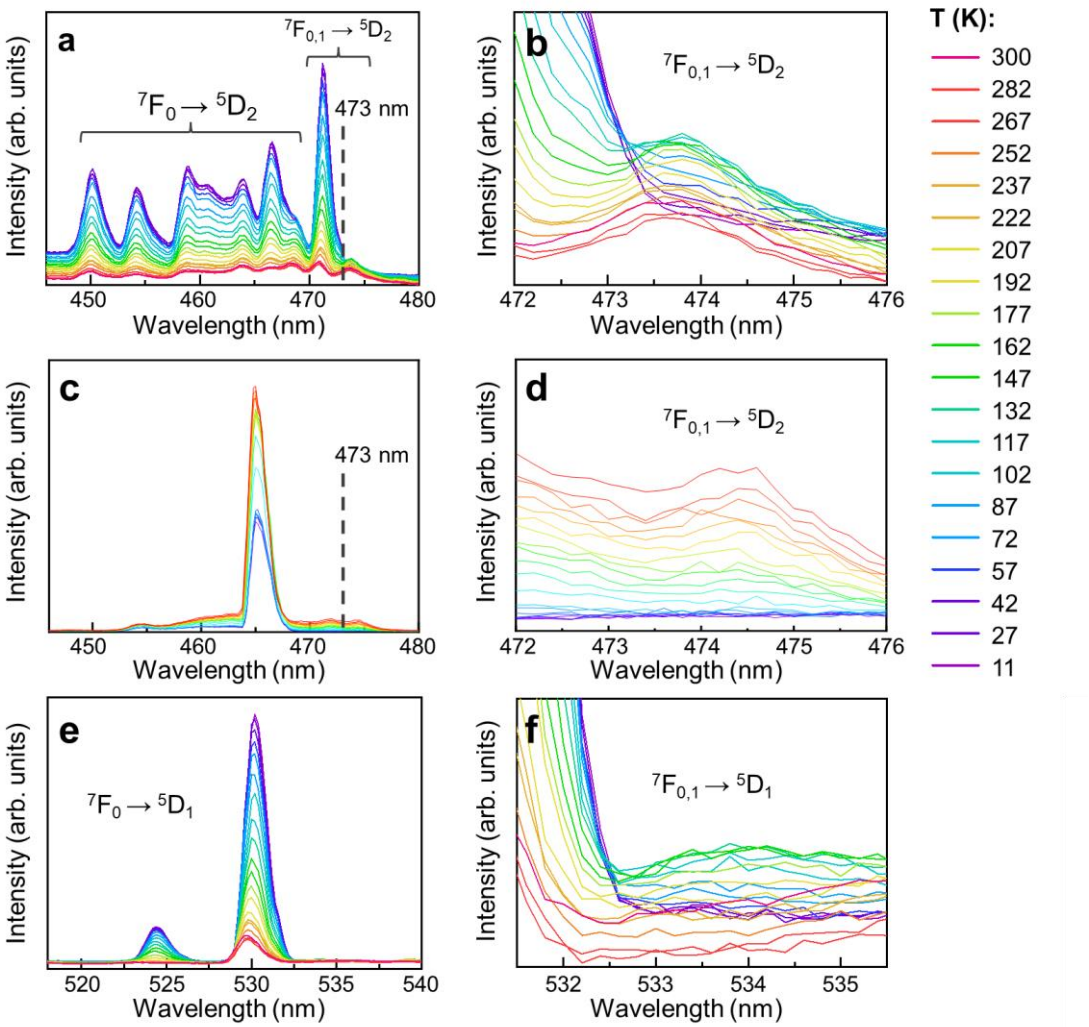

Figure S3. Excitation spectra as a function of the temperature for (a) $BaTiO_3:Eu^{3+}$ [10] and (c) $CaTiO_3:Eu^{3+}$ in the 445 – 480 nm range. Off-resonance excitations are magnified in plots (b) and (d). For clarification purposes, the $^7F_0 \rightarrow {}^5D_1$ (e) and $^7F_1 \rightarrow {}^5D_1$ (f) transitions in $BaTiO_3:Eu^{3+}$ are also represented. Panels (a) and (e) were adapted with permission from *Arnab De, Vivek Dwij, Vasant Sathe, M.A. Hernández-Rodríguez, Luís D. Carlos, Rajeev Ranjan, Synergistic use of Raman and photoluminescence signals for optical thermometry with large temperature sensitivity, Phys. B: Condens. Matter. 626 (2022) 413455, © 2022 Elsevier Science B.V.*

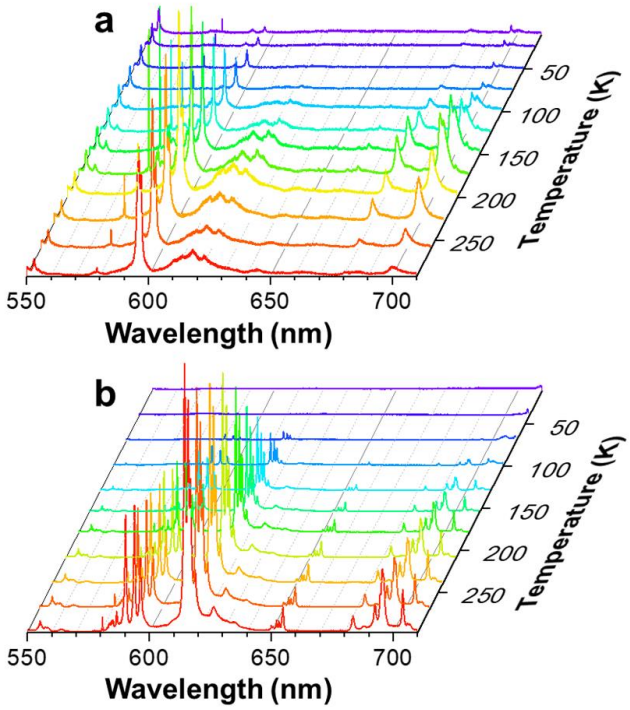

Figure S4. Temperature dependence of the emission spectra of (a) $BaTiO_3$:0.5Eu and (b) $CaTiO_3$:0.5Eu when excited off-resonance with a laser source at 532 nm.

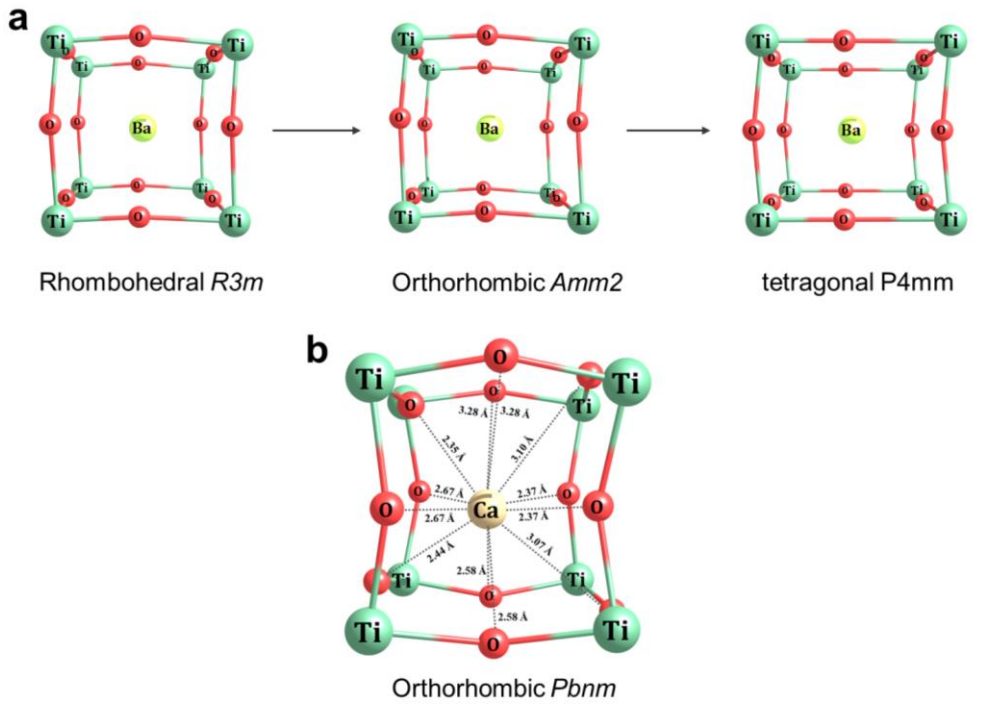

Figure S5. (a) Local symmetry close to a center of inversion of the Ba^{2+} ion (or Eu^{3+}) when the $BaTiO_3$ undergo phase transitions below 300 K. (b) Ca–O distances in $CaTiO_3$ structure showing that the Ca^{2+} site is slightly displaced from a center of inversion. Structures retrieved from references [12,13].

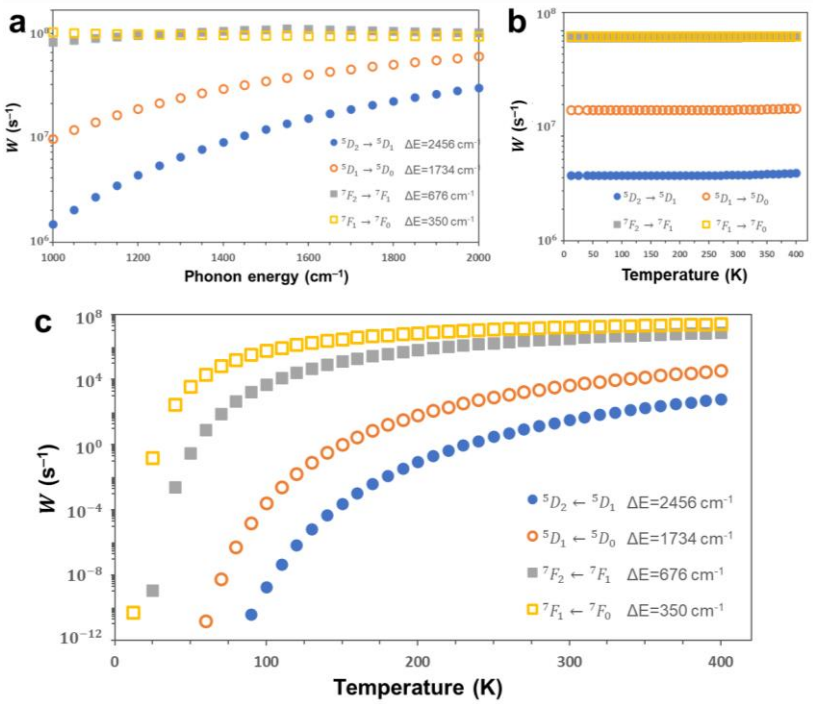

Figure S6. (a) Multiphonon decay rates (in s^{-1}) as a function of the mean phonon energy $\hbar\bar{\omega}$ (in cm^{-1}). Multiphonon decay (b) and absorption (c) rates as a function of temperature (in K) considering $\hbar\bar{\omega} = \mathbf{1200}$ cm^{-1}. The Huang-Rhys factor S = 0.16 was used in calculations [11].

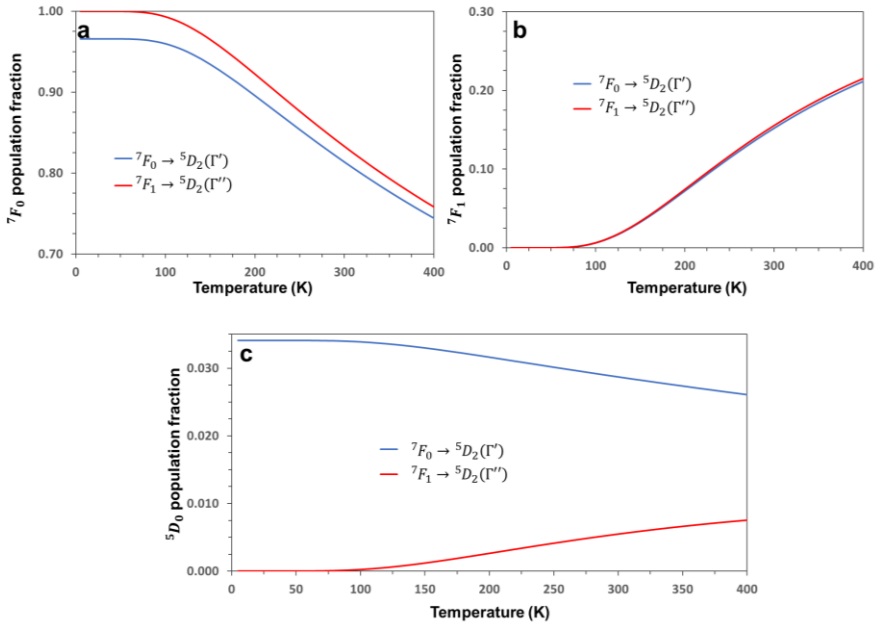

Figure S7. Population fraction in the steady-state regime of the (a) $^7F_0$, (b) $^7F_1$, and (c) $^5D_0$ levels. The blue curves represent simulations where only the $\boldsymbol{^7F_0 \rightarrow {}^5D_2(\Gamma')}$ are considered, *i.e.*, only the GSA process ($\boldsymbol{\delta_{F0} = 1}$ and $\boldsymbol{\delta_{F1} = 0}$ are used in the rate equations model). The red curves consider only the $\boldsymbol{^7F_1 \rightarrow {}^5D_2(\Gamma'')}$ transition as excitation, *i.e.*, ESA process ($\boldsymbol{\delta_{F0} = 0}$ and $\boldsymbol{\delta_{F1} = 1}$ are used in the rate equations model).

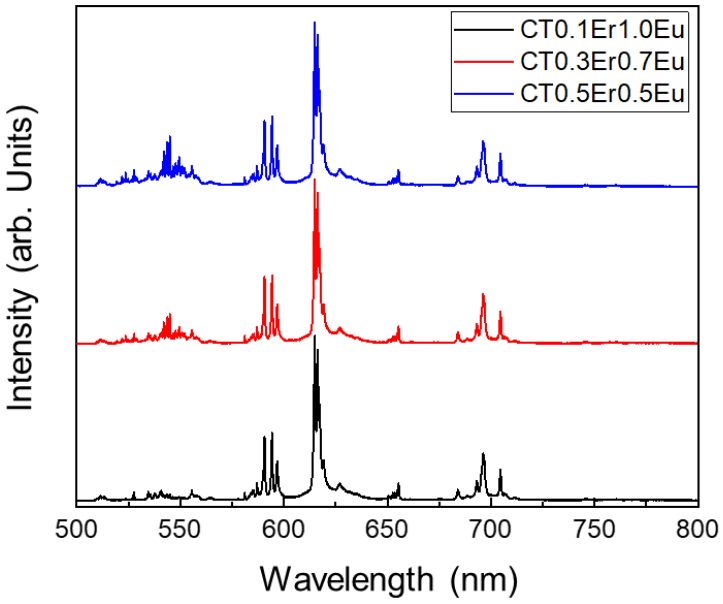

Figure S8. Room temperature emission spectra of Er^{3+} and Eu^{3+} co-doped $CaTiO_3$ under 473 nm excitation (laser source) with varying Eu^{3+} and Er^{3+} concentrations (Er/Eu = 0.1/1.0, 0.3/0.7, 0.5/0.5).

S4. Tables

Table S1. Coefficients of the intermediate coupling scheme wavefunctions for the Eu^{3+} ion [1].

LS state		Coefficients					
n	φ_n	$^7F_0$	$^7F_1$	$^7F_2$	$^5D_0$	$^5D_1$	$^5D_2$
1	^{7}F	0.9680	0.9742	0.9819	-0.2381	-0.2096	-0.1624
2	^{5}G	0	0	-0.0025	0	0	-0.0155
3	^{5}S	0	0	0.0005	0	0	0.0037
4	^{5}G'	0	0	-0.0147	0	0	0.0014
5	^{5}P	0	-0.0027	-0.0035	0	0.0012	-0.0054
6	^{5}G''	0	0	0.0172	0	0	0.0038
7	^{5}D	0.0016	0.0052	0.0108	-0.1969	-0.2066	-0.2104
8	^{5}H	0	0	0	0	0	0
9	^{5}D'	0.1659	0.1472	0.1161	0.6893	0.7162	0.7456
10	^{5}H'	0	0	0	0	0	0
11	^{5}D''	-0.1815	-0.1645	-0.1353	-0.5390	-0.5561	-0.5742
12	^{5}I	0	0	0	0	0	0
13	^{5}F	0	0.0263	0.0452	0	-0.0536	-0.0888
14	^{5}I'	0	0	0	0	0	0
15	^{5}F'	0	0.0162	0.0289	0	-0.0373	-0.0724
16	^{5}K	0	0	0	0	0	0
17	^{5}L	0	0	0	0	0	0

Table S2. Values of squared reduced matrix elements used in the calculations of radiative rates. The values of $\langle \psi J \| U^{(\lambda)} \| \psi' J' \rangle^2$ were taken from references [9,14] and $\langle \psi J \| \mathbf{L} + g_S \mathbf{S} \| \psi' J' \rangle^2$ were calculated as presented in section *S1. Orbital and Spin matrix elements*.

Transition	$\langle \psi J \| U^{(2)} \| \psi' J' \rangle^2$	$\langle \psi J \| U^{(4)} \| \psi' J' \rangle^2$	$\langle \psi J \| U^{(6)} \| \psi' J' \rangle^2$	$\langle \psi J \| \mathbf{L} + g_S \mathbf{S} \| \psi' J' \rangle^2$
$^7F_0 \leftrightarrow {}^7F_1$	0	0	0	9.820
$^7F_0 \leftrightarrow {}^7F_2$	0.1374	0	0	0
$^7F_0 \leftrightarrow {}^5D_1$	0	0	0	0.027
$^7F_0 \leftrightarrow {}^5D_2$	0.0008	0	0	0
$^7F_1 \leftrightarrow {}^7F_2$	0.0518	0	0	21.316
$^7F_1 \leftrightarrow {}^5D_0$	0	0	0	0.116
$^7F_1 \leftrightarrow {}^5D_1$	0.0025	0	0	0.941×10^{-3}
$^7F_1 \leftrightarrow {}^5D_2$	0.0001	0	0	0.458×10^{-2}
$^7F_2 \leftrightarrow {}^5D_0$	0.0032	0	0	0
$^7F_2 \leftrightarrow {}^5D_1$	0	0	0	2.008
$^7F_2 \leftrightarrow {}^5D_2$	0.0018	0.0015	0	2.432
$^7F_4 \leftrightarrow {}^5D_0$	0	0.0023	0	0
$^7F_4 \leftrightarrow {}^5D_1$	0	0.0028	0	0
$^7F_4 \leftrightarrow {}^5D_2$	0.0020	0.0003	0	0
$^5D_0 \leftrightarrow {}^5D_1$	0.3782	0.1343	0.1575	4.911
$^5D_0 \leftrightarrow {}^5D_2$	0.0142	0	0	0
$^5D_1 \leftrightarrow {}^5D_2$	0.0122	0	0	9.544

Table S3. Integrated areas of the Eu^{3+} $^5D_0 \rightarrow {}^7F_2$ ($S_{0\rightarrow2}$) and Eu^{3+} $^5D_0 \rightarrow {}^7F_4$ ($S_{0\rightarrow4}$) transitions with the $S_{0\rightarrow1}$ set to 1. Values of Ω_λ ($\lambda = 2, 4$) for Eu^{3+} doped $BaTiO_3$ and $CaTiO_3$ hosts.

Host	$S_{0\rightarrow2}$	$S_{0\rightarrow4}$	Ω_2 (10^{-20} cm^2)	Ω_4 (10^{-20} cm^2)
$CaTiO_3$	2.26	1.41	3.06	3.90
$BaTiO_3$	0.90	1.58	1.17	4.20

Table S4. Calculated radiative rates $A_{J\to J'} = A^{ED} + A^{MD}$, where A^{ED} and A^{MD} stand for the rates (in units of s^{-1}) from the electric dipole and magnetic dipole, respectively. n_r = 2.3 ($CaTiO_3$) and 2.4 ($BaTiO_3$) were considered in the calculations [6,7].

Phosphor	Transition	A^{ED} (s^{-1})	A^{MD} (s^{-1})	$A_{J\to J'}$ (s^{-1})
$CaTiO_3$:Eu^{3+}	$^5D_2\to{}^7F_0$	47.64	0	47.64
	$^5D_2\to{}^7F_1$	5.67	2.83	8.50
	$^5D_2\to{}^7F_2$	190.84	1.36×10^3	1.56×10^3
	$^5D_2\to{}^7F_4$	92.96	0	92.96
	$^5D_1\to{}^7F_0$	0	20.54	20.54
	$^5D_1\to{}^7F_1$	163.03	0.67	163.70
	$^5D_1\to{}^7F_2$	0	1.28×10^3	1.28×10^3
	$^5D_1\to{}^7F_4$	151.98	0	151.98
	$^5D_0\to{}^7F_1$	0	184.92	184.92
	$^5D_0\to{}^7F_2$	413.62	0	413.62
	$^5D_0\to{}^7F_4$	266.69	0	266.69
$BaTiO_3$:Eu^{3+}	$^5D_2\to{}^7F_0$	21.54	0	21.54
	$^5D_2\to{}^7F_1$	2.56	3.22	5.78
	$^5D_2\to{}^7F_2$	167.00	1.55×10^3	1.72×10^3
	$^5D_2\to{}^7F_4$	54.28	0	54.28
	$^5D_1\to{}^7F_0$	0	23.34	23.34
	$^5D_1\to{}^7F_1$	73.70	0.76	74.46
	$^5D_1\to{}^7F_2$	0	1.45×10^3	1.45×10^3
	$^5D_1\to{}^7F_4$	193.52	0	193.52
	$^5D_0\to{}^7F_1$	0	2.10×10^2	2.10×10^2
	$^5D_0\to{}^7F_2$	186.99	0	186.99
	$^5D_0\to{}^7F_4$	339.58	0	339.58

References

[1] G.S. Ofelt, Structure of the f^6 Configuration with Application to Rare-Earth Ions, J. Chem. Phys. 38 (1963) 2171–2180. https://doi.org/10.1063/1.1733947.

[2] I.P. Assunção, A.N. Carneiro Neto, R.T. Moura, C.C.S. Pedroso, I.G.N. Silva, M.C.F.C. Felinto, E.E.S. Teotonio, O.L. Malta, H.F. Brito, Odd-Even Effect on Luminescence Properties of Europium Aliphatic Dicarboxylate Complexes, ChemPhysChem. 20 (2019) 1931–1940. https://doi.org/10.1002/cphc.201900603.

[3] K. Binnemans, Interpretation of europium(III) spectra, Coord. Chem. Rev. 295 (2015) 1–45. https://doi.org/10.1016/j.ccr.2015.02.015.

[4] J.-C.G. Bünzli, On the design of highly luminescent lanthanide complexes, Coord. Chem. Rev. 293–294 (2015) 19–47. https://doi.org/10.1016/j.ccr.2014.10.013.

[5] G.F. de Sá, O.L. Malta, C. de Mello Donegá, A.M. Simas, R.L. Longo, P.A. Santa-Cruz, E.F. da Silva, Spectroscopic properties and design of highly luminescent lanthanide coordination complexes, Coord. Chem. Rev. 196 (2000) 165–195. https://doi.org/10.1016/S0010-8545(99)00054-5.

[6] K. Ueda, H. Yanagi, R. Noshiro, H. Hosono, H. Kawazoe, Vacuum ultraviolet reflectance and electron energy loss spectra of $CaTiO_3$, J. Phys. Condens. Matter. 10 (1998) 3669–3677. https://doi.org/10.1088/0953-8984/10/16/018.

[7] S.H. Wemple, M. Didomenico, I. Camlibel, Dielectric and optical properties of melt-grown $BaTiO_3$, J. Phys. Chem. Solids. 29 (1968) 1797–1803. https://doi.org/10.1016/0022-3697(68)90164-9.

[8] A.N. Carneiro Neto, E.E.S. Teotonio, G.F. de Sá, H.F. Brito, J. Legendziewicz, L.D. Carlos, M.C.F.C. Felinto, P. Gawryszewska, R.T. Moura Jr., R.L. Longo, W.M. Faustino, O.L. Malta, Modeling intramolecular energy transfer in lanthanide chelates: A critical review and recent advances, in: J.-C.G. Bünzli, V.K. Pecharsky (Eds.), Handb. Phys. Chem. Rare Earths, Vol. 56, Elsevier, 2019: pp. 55–162. https://doi.org/10.1016/bs.hpcre.2019.08.001.

[9] W.T. Carnall, H. Crosswhite, H.M. Crosswhite, Energy level structure and transition probabilities in the spectra of the trivalent lanthanides in LaF_3, Argonne, IL, United States, 1978. https://doi.org/10.2172/6417825.

[10] A. De, V. Dwij, V. Sathe, M.A. Hernández-Rodríguez, L.D. Carlos, R. Ranjan, Synergistic use of Raman and photoluminescence signals for optical thermometry with large temperature sensitivity, Phys. B Condens. Matter. 626 (2022) 413455.

https://doi.org/10.1016/j.physb.2021.413455.

[11] S. Som, A.K. Kunti, V. Kumar, V. Kumar, S. Dutta, M. Chowdhury, S.K. Sharma, J.J. Terblans, H.C. Swart, Defect correlated fluorescent quenching and electron phonon coupling in the spectral transition of Eu^{3+} in $CaTiO_3$ for red emission in display application, J. Appl. Phys. 115 (2014) 193101. https://doi.org/10.1063/1.4876316.

[12] R. Ali, M. Yashima, Space group and crystal structure of the Perovskite $CaTiO_3$ from 296 to 1720 K, J. Solid State Chem. 178 (2005) 2867–2872. https://doi.org/10.1016/j.jssc.2005.06.027.

[13] M.B. Smith, K. Page, T. Siegrist, P.L. Redmond, E.C. Walter, R. Seshadri, L.E. Brus, M.L. Steigerwald, Crystal Structure and the Paraelectric-to-Ferroelectric Phase Transition of Nanoscale $BaTiO_3$, J. Am. Chem. Soc. 130 (2008) 6955–6963. https://doi.org/10.1021/ja0758436.

[14] W.T. Carnall, P.R. Fields, K. Rajnak, Electronic Energy Levels of the Trivalent Lanthanide Aquo Ions. IV. Eu^{3+}, J. Chem. Phys. 49 (1968) 4450–4455. https://doi.org/10.1063/1.1669896.